Open Source Tendon-driven Continuum Mechanism: A Platform for Research in Soft Robotics

Bastian Deutschmann, Jens Reinecke, and Alexander Dietrich

***Abstract*— This paper introduces a tendon-driven continuum mechanism platform for research on design, modeling, state estimation, and control of this challenging robotic component envisioned as highly versatile and mechanically robust joint for future robotic systems. To propel the corresponding research areas, a common platform is presented for benchmarking and transferability of results, approaches, and designs among different research groups. The proposed mechanical design including all components is open source, whereas electronics and actuation are off-the-shelf. Research groups are enabled to build up their own system as all relevant CAD-files and assembly instructions are made accessible through GitHub. With that, a fundamental goal in research is achieved and will push continuum joints towards real application scenarios for future soft robots.**

I. INTRODUCTION

Research within the soft robotics community is often performed on hardware which is available to one research group or institution only. Common platforms are not well established. As a result, models and their parameters, configurations, state estimation methods, or control algorithms treat specific problems associated with their underlying hardware, but the transferability of the results among platforms is limited. To benchmark and compare methods and algorithms in this field, common platforms can provide the means for streamlined developments, evaluations, validations, and effective comparisons with the state of the art. Furthermore, the underlying open-source concept in such platforms allows direct access to all necessary information in order to overcome well-known design problems, typical manufacturing issues, and common control challenges. The barrier to entry is facilitated for researchers and facilities who are new to the field, while active exchange and continuous improvements of existing solutions through experienced involved researchers can foster the continuous technological progress. All these efforts in terms of open source, transferability, and reproducibility go in hand with current trends in the robotics community [3].

With the rise of light-weight robotic arms, a role model development has happened in the past. In the late 90s, only a few research institutions built their own manipulators to perform research on and with them. Nowadays, due to the availability of such robots through commercialization, e.g., the KUKA-LWR [1] or the UR 3 [28] to name a few, institutions which couldn't afford the resources, can now perform research in this area.

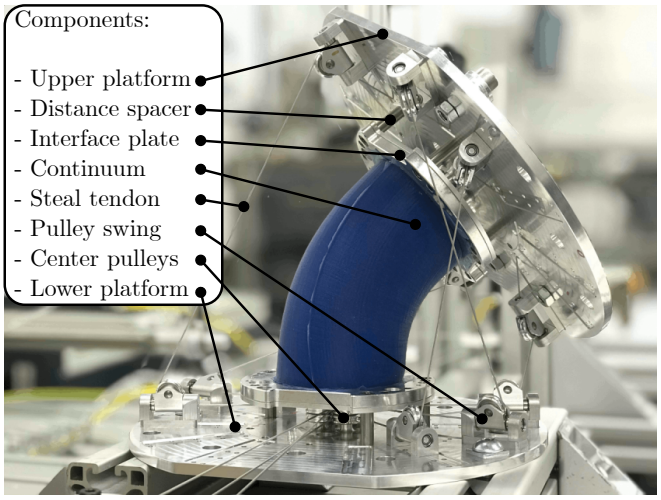

Fig. 1: Testbed of the open source tendon-driven continuum mechanism. In this setup, six tendons and the corresponding actuators are used.

Several open source robotic platforms such as [2] are available to exploit the synergies of parallel research. One of the first attempts in this direction was conducted by Willow Garage more than ten years ago, with their wheeled humanoid PR2 [6] and the promotion of ROS. The robotic platforms have been given to several research institutions in the US for free. Yet, the mechatronic hardware components were not open source. Other more recent projects aim to make quadrupedal locomotion systems and humanoid robots available to the community. Among them are Mini-Pupper [26] or the Poppy project [22].

In terms of open source platforms for soft robotics, a popular instrument is the Soft-Robotics Toolkit [29]. In its early stages, this toolkit was comprised of a manual to build and control a single pneumatic actuator [14]. By now, a variety of actuation types of pneumatic actuators can be selected, including instructions about their manufacturing process, details about their modeling and possible sensors that can be included. Another work is propelling research in continuum systems for

The authors are with the Institute of Robotics and Mechatronics of the German Aerospace Center (DLR) bastian.deutschmann@dlr.de

Bastian Deutschmann and Jens Reinecke equally contributed to this work.

surgical applications. ENDO [5] is a slender tendon-driven robot, which can be built via 3D printing devices. The total cost, including the actuation and control unit, amounts to approximately 100 USD making it affordable for research institutions and universities.

The motivation of the current tendon-driven continuum mechanism is to be integrated in larger robotic systems than the typically very thin surgical catheter-like systems [4]. Similar joint designs in other hardware systems are, for example, finger joints in robotic multi-fingered hands [20], humanoid [25] and quadrupedal spines [31] or full manipulators [19] for which several mechanisms are serially attached to each other.

The contribution of this paper is twofold. The primary focus is the introduction of an open source research platform to the soft robotics community including a justification of the proposed design. Here, we focus on mechanical reliability and robustness which is supported by an experiment-based interface design and initial experiments of the fully assembled platform. All components including manufacturing guidelines are available on GitHub [21]. The second focus is the experimental investigation of the interface between the hard and the soft component which will be of help to other research engineers designing similar robotic systems.

The paper is organized as follows. In Section II, the mechanical design is presented and key features are discussed. Afterward, Section III presents initial experiments to demonstrate the potential of the open source experimental platform. In Section IV a discussion about short and long term research areas, which need to be addressed to push tendon-driven continuum mechanisms towards real robotic applications, are discussed. The paper concludes with a summary of the presented work in Section V.

II. Design & Manufacturing of the open-source tendon-driven continuum mechanism

A tendon-driven continuum mechanism consists of a continuously deformable structure in between two rigid platforms [10]. The testbed proposed here is depicted in Fig. 2.

A. Upper and lower platform

The upper and lower platform are identical as shown in Fig. 2. They were designed to enable the investigation of the influence of the tendon routing on the workspace of the mechanism. Therefore, up to eight actuated tendons can be routed in different configurations from the lower to the upper platform. Along three channels in all four quadrants of the platform, tendon pulleys can be placed. In total, 36 different locations (4 quadrants x 3 channels x 3 different positions per channel = 36) exist where a tendon pulley can be mounted. In the center four bearing mounts are located to route the tendons from their pulley mounting point to the platform center and then to the actuation. As a maximum of eight tendons where envisioned, two pulleys fit on top of each other at each bearing mount.
In our testbed, the platform is manufactured from aluminum. However, if more compliant continuum structures are used and the tendon loading is reduced, 3D-printed platforms instead of aluminum is feasible as well. To further enable varying geometries and tendon routings, spacers of different height can be utilized with which the interface plates and the platforms are combined.

B. Silicone structure

The silicone structure is molded from Dragon Skin [15]. In the first version of the testbed the structure possesses a cylindrical cross section. Corresponding molds are 3D-printed, see Fig. 3, and can be firmly connected with the interface plates using screws. A release agent [16] from dragon skin is used to cover the inside of the molds to enable an easy release of them when curing of the silicone is finished.

To establish a mathematical model, the stiffness properties are important. For mechanical rigorous formulations, e.g. [13], [11], the Young's modulus is of major importance. Four experiments are carried out in order to grasp the Young's modulus of the silicone within a compression test setup using the Zwick compression testing machine. In the left plot of Fig. 4, two specimens are tested with the same geometrical property (length 9.5 cm, diameter 6.2 cm) but molded from Dragon Skin shore 20A and shore 30A. In the right plot of Fig. 4, two specimens of Dragon Skin shore 30A are tested possessing different length but the same diameter (here 3 cm). The results are depicted in Fig. 4. A nonlinear material behavior can be observed in all measurements. As an example, a Neo-Hookian material [11] law is used for the fitting. To show the amount of non-linearity, a linear Hookian material law is given in the left experiment implying that the material nonlinearity is not large within the measured displacement.
In summary, the experimentally optained Young's Modulus of Dragon Skin 30A is of comparable magnitude despite the different geometric properties of the test specimens. While a speciment with diameter of 29mm and a lenght of 40mm posses $E = 901120\ N/m^2$, a specimen with a diameter of 62mm and a length of 95mm posses a $E = 1001100\ N/m^2$. However, for the aforementioned rigorous models, it is therefore recommended to identify the Young's modulus in for the individual geometrie.

C. Interface between hard & soft material

A firm interconnection of the hard and soft material component is crucial. In case of failure of this interface, the continuum mechanism falls apart and its functionality is lost. The connection towards the soft

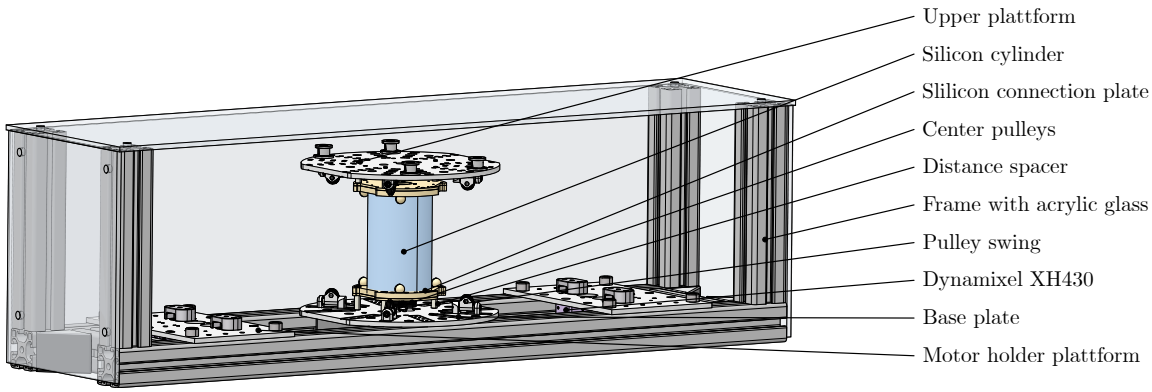

Fig. 2: Overview of the proposed open source tendon-driven continuum mechanism with all involved components.

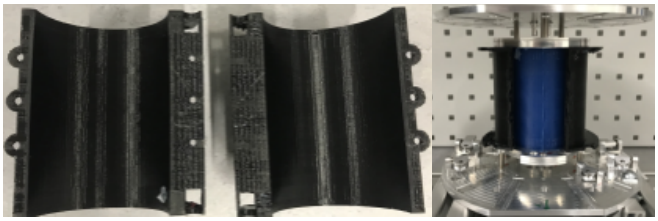

Fig. 3: Left: 3D printed molds to manufacture a cylindrical silicone structure. Right: Illustration of the molds onto the continuum mechanism.

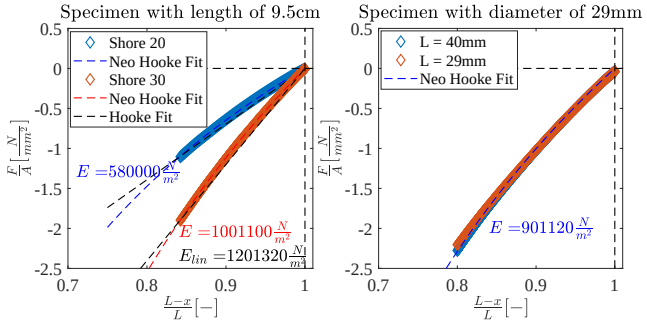

Fig. 4: Compression test performed with the ZwickRoell®axial compression machine. Left: Two cylindrical continuum structures including the interface plate designed in Sec. II-C are loaded axially whereas axial force and the corresponding displacement are measured. Left: Specimens with the same geometric properties and different shore hardness are tested. Right: Specimens with the same silicone but with different geometric properties are displayed.

material is realized by an interface plate which can further be mounted to adjacent components, in our case the upper and lower platform. The requirements of the interface plate are as follows:

- at maximum 8 mm thick,
- easy to manufacture,
- withstand high loadings; in critical loading cases, it is expected that the continuum will be deformed such that the upper platform is turned 180° w.r.t. the lower platform,
- accurate positioning of the continuum structure w.r.t. its mounting is required.

To fulfill the requirements and establish a firm

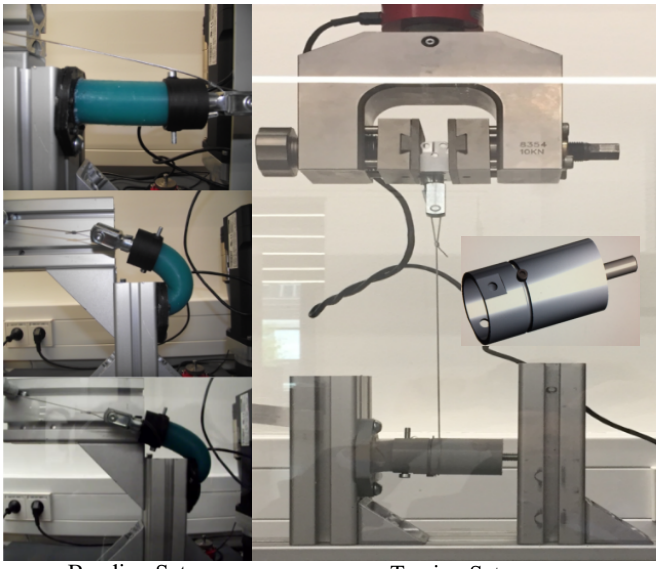

Fig. 5: Two experimental setups within a ZwickRoell® [32] axial testing machine. The two setups investigate different interface candidates with respect to their ability to withstand excessive load cases. Left: bending setup. Right: torsional setup.

connection that can withstand extensive loading, an experimental test procedure has been carried out. The design of the mechanism and its tendon routing impose three major loading conditions: axial compression, bending, and torsion. Axial compression does not affect the loading on the interface between hard and soft, however bending and torsion do. To account for it, two experimental setups including a Zwick axial force testing machine [32] were designed. The first setup investigates the ability of the hard-soft interface to withstand excessive bending loads, see Fig. 5 (left), and the second one investigates the torsional loading case, see Fig. 5 (right).

As a hard material, aluminum and PLA (3D-printer material) is used. As soft material, silicone from Dragon Skin [15] is deployed. We have experimentally investigated adhesion and form closure in eleven different interface designs to interconnect the soft and hard

component. Six of them use adhesion to establish proper interface connections, Model 1-6, see Fig. 6, whereas Model 7-11 use form closure with different interface geometries.

The following experimental procedure has been performed for both loading cases and for all eleven interface models in combination with both two hard materials. It covers bending until nominal loading, i.e., when the upper platform is turned 180° in bending or torsion. This loading condition is statically held for 300 s. Afterwards, a cyclic loading of twenty cycles is performed whereas in each cycle, the nominal loading is reached. The last test involves the load until failure.

1) Bending: The full results can be seen in Tab. I where all pairings are listed and the failure load measured by the Zwick machine is given. Furthermore, the experimental curves in Fig. 7 for two competing candidates using adhesion and four competing candidates using form closure are given. In summary, the majority of the adhesion interface types failed in the very early stages, except for Model 5 A and Model 6 P (displayed in the curves). Furthermore, we can see that the interfaces using PLA as a hard material are softer in terms of stiffness compared to the aluminum ones. This can be seen by comparing e.g. Model-8 A and P in the first plot of Fig. 7 which leads to the conclusion that the PLA is bending itself. In terms of failure, however, no difference between PLA and aluminum can be seen in the third plot by comparing the same models for aluminum and PLA. Thin connections of the soft materials to the hard materials, as in Model 10, tend to fail by material damage whereas larger cross-sections (Model 8 or 9) in the form closures are able to withstand the loading.

It needs to be noted that an irregular quality of the interface connection was observed when using silicone glue. This type of glue releases acetic when curing and therefore requires humidity in the surrounding air. Especially for connecting silicone with the glue in the liquid stage, not enough humidity had been present due to tight moldings which resulted in an insufficient curing process. Moreover, the form closure interfaces were more convenient in the molding process compared to the adhesion candidates as no additional treatments were required.

The most promising interface candidates have been Model 8 and Model 9 as they withstood all tests and their failure loads have been the largest.

2) Torsion: For the torsional experiment, Model 8, Model 9 (due to their superior performance in the bending experiment), Model 10 and a modified version of Model 8 and 9 with a hexagonal cavity shape in the interface plate have been investigated. All models have been tested for both, PLA and aluminum, as a hard material. Table I reveals similar measured failure loads for all candidates, except for Model 10. Here, the small tunnels that connect the soft and the hard material slowly broke during the cyclic loading which can be seen in Fig. 7 in a continuously decreasing torsional torque. Furthermore, Fig. 7 shows that although Model 8 and Model 9 perform well in the torsional test and break at high loadings (after passing the static and the cyclic loading test), slipping is present. At high loadings, the maximum torque remains almost constant whereas the angle still increases. To counteract slippage, the circular cavities of Model 8 and 9 have been modified to have a hexagonal shape to counteract slippage, see Fig. 6 on the right. As illustrated in Fig. 7, models with hexagonal shape exhibit even higher failure loads whereas slippage is not present.

3) Summary: In Section II-C, different alternative interface designs to firmly attach the hard and soft component of the continuum mechanism have been experimentally tested. Model 8 with hexagonal cavity design performed at best in the bending and torsion experiment and is therefore chosen for the testbed platform. The final design is depicted in Fig. 2.

D. Tendon guiding

The tendons are guided from the lower to the upper platform by rotatable pulleys, called pulley swings see Fig. 8. They can rotate about an axis perpendicular to the pulley axis and ensure that the tendons will not fall off the pulley when large motions of the upper platform occur.. The pulleys are equipped with bearings to reduce friction during the motion of a tendon.

To enable rotational actuators, such as the proposed Dynamixel XH430 [27], a motor winch is designed, see Fig. 8 (right). It enables to twirl the tendon around the winch and a radial hole in the winch is incorporated to clamp the tendon and ensure a firm attachment. By twirling the tendon on the winch by multiple windings, the resulting friction (belt friction) ensures that the clamp on the tendon does not need to withstand excessive loading.

The winches can be mounted to the upper platform using M6 screws and a corresponding nut. This is done to clamp the tendons in the upper platform, see Fig. 1.

E. Actuation possibilities

When building the tendon-driven continuum mechanism, we envisioned to have two types of possible actuation: Linear actuators and rotational actuators. However, also passive loads can be applied by simply putting weights at the free tendon end or directly at the upper platform without using tendons, see Fig. 9 for an illustration. The experiments in the next chapter are performed using linear actuators from Linmot® [18] as they are equipped with several different sensors, especially tendon position and tension sensors to enable more accurate static and dynamic experiments. In the bottom of Fig 9, the experimental setup with the linear motors is given.

For the open source project, rotational off-the-shelf actuators with software interface from Robotis,

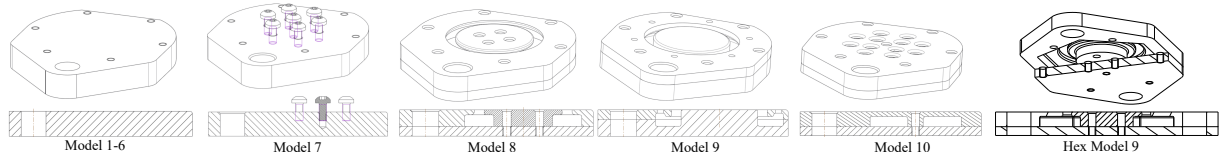

Fig. 6: Eleven different interface types manufactured for the hard materials, PLA and aluminum. Model 1-6 is a flat surface to test adhesion of the silicone and the hard material. For Model 1-3, the silicone is connected with the hard material within the liquid state. Here, Model 1 uses no additional treeatment, Model 2 uses silicone-glue [30] and Model 3 uses silicone-glue and a primer [17]. For Model 4-6, the silicone is connected in rigid state whereas again, Model 4 uses no additional treatment, Model 5 uses silicone-glue and Model 6 uses silicone-glue and a primer. Model 7 uses screws in order to achieve form closure whereas the silicone is molded around the screws to achieve form closure. Model 8 uses a circular belt to establish form closure, whereas Model 9 uses a circular hook. Model 10 is manufactured to have several tunnels through which the silicone can flow during the molding process into a cavity within the interface plate. Model 11 (Hex Model 8 / 9) uses a hexagonal shape in coordination with the ring/hook geometry of Model 8/9.

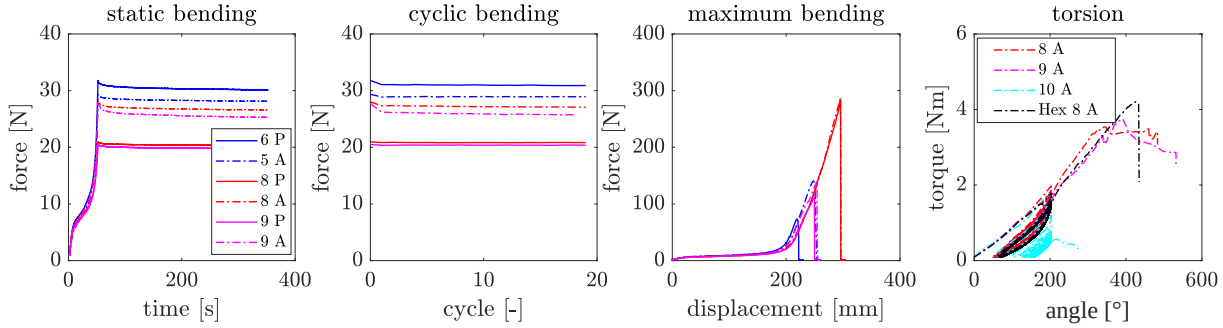

Fig. 7: Static bending: Measured loading (linear force of the Zwick machine) for the bending experiment. The different candidates are loaded until the top plate is bent to 180° i.e. the nominal loading. Afterwards, the loading is held for 300 s. Cyclic bending: The candindates are loaded and unloaded 20 times to the nominal loading. The curves show the measured force of the Zwick machine at each nominal loading point. Maximum bending: The maximum bending experiment covers the loading of each candidate until failure, which means that either the interface or some other parts fail. As mentioned earlier, each candidate failed at the interface. Torsion: Measured torsional torque w.r.t. the torsional angle for four candidates. Similar to the bending experiment, Model 8 and 9 exhibit the highest failure load, however tend to slip. The adapted hexagonal cavity in Model 8 (and also Model 9) prevents this slippage.

TABLE I: Experimental results for the bending and torsional loading case for all investigated pairing of interface types, PLA and aluminum as a hard material. Model 4 (no interface treatment, soft material in rigid state is directly placed on the interface) is excluded in the Table as it could not withstand any loading (0 N until failure)

	PLA										Aluminum									
	Adhesion					Form closure					Adhesion					Form Closure				
Loading	1	2	3	5	6	7	8	9	10	Hex	1	2	3	5	6	7	8	9	10	Hex
Nominal [N]	9	3	10			8					7		21		23	10				
Static [N]									21			19								
Cyclic [N]				26																
Failure [N]					73		284	112						127			287	140	93	
Torsion [Nm]							3.6	3.6		3.8							3.5	3.7	1	4.1

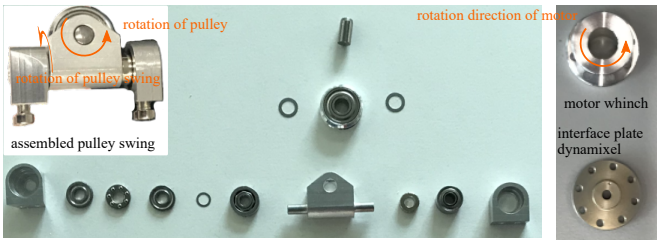

Fig. 8: Parts for the tendon guiding. Left: Components and assembled pulley swing designed for large tendon motions, high tensional loading and low tendon path friction. Right: Motor winch for the Dynamixel®XH430 actuators to transfer the rotational motion of the motor into a longitudinal motion of the tendon.

Dynamixel®XH430 [27] are utilized. The software allows them to be operated via many programming languages e.g., Python, C, or Matlab/Simulink. The API is also open source and provided by the manufacturer [27].

Fig. 10 shows a setup including Dynamixel actuation. Therefore, an actuation holder plate was designed to mount the Dynamixel®, see Fig. 2. At the output shaft, the winches from Fig. 8 are used to pull the tendons. The Dynamixel®servo is available in many variations, it can be ordered with different gear ratios (210 and 350), operating voltages (12V and 24V) and motors (Maxxon®or lower quality), but the mechanical interface is suitable in each of these versions.

To drive the Dynamixels®, one can use the Controller OpenCR 1.0 board or the simple U2D2 communication module. The controller board offers also a variety of interfaces and a sensor for orientation estimation MPU9250.

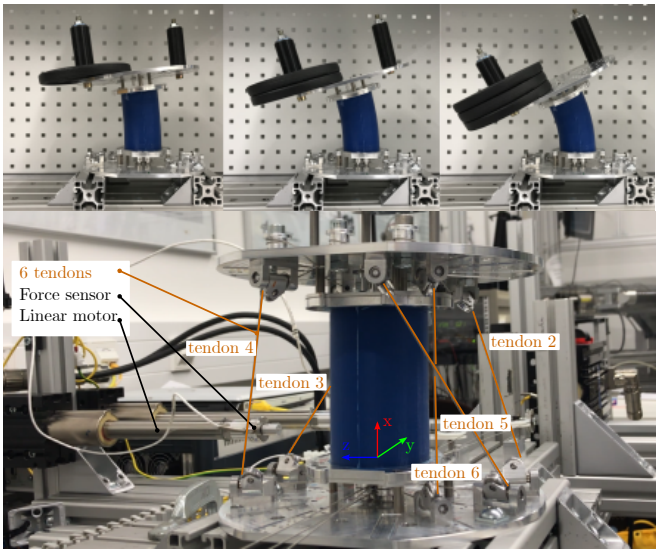

Fig. 9: Top row: Experiments without tendons to illustrate the ease of deforming the system and perform experiments. Bottom: Testbed actuated by linear motors from Linmot®.

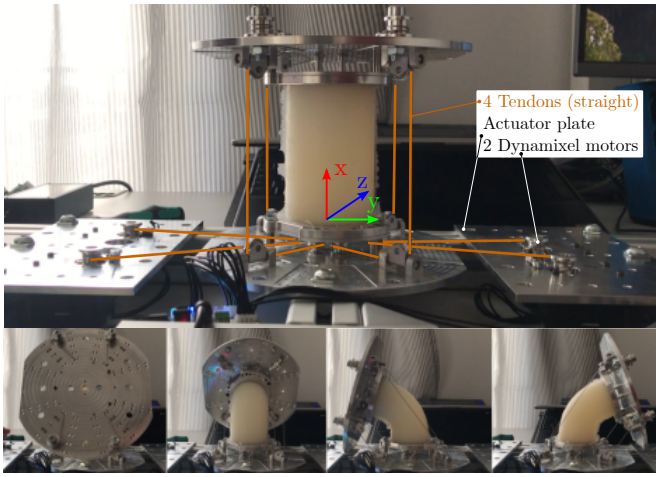

Fig. 10: Open source tendon-driven continuum robot equipped with four tendons and actuators.

III. Experiments: Characterization of the motion capabilities

The aim of this section is to exemplify the motion capabilities of the proposed testbed for two tendon configurations.

In the first, quantitative assessment, four tendons are used and actuated by four Dynamixel XH430 motors, see Fig. 10. The routing of the tendons is chosen identical in the lower and upper platform to be initially straight and 90° separated. With that, a (majorly) bending motion in two directions is induced when pulling one or two tendons. In Fig. 10, a symmetric bending motion can be observed with an angle of 85° to all the sides, measured with the help of a digital spirit level.

The second test is performed with the continuum mechanism using six tendons within the setup equipped with six linear motors. The six tendons are arranged

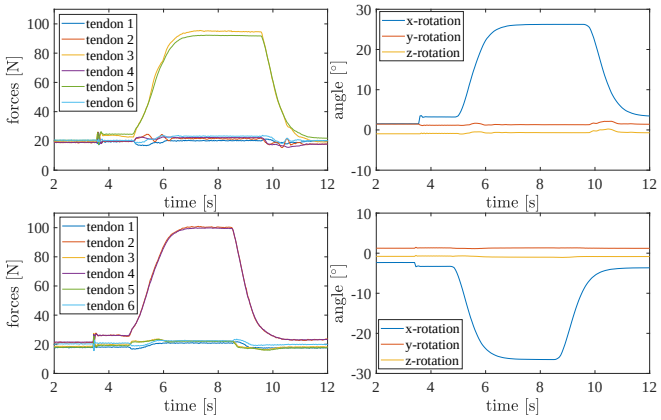

Fig. 11: Positive (top) and negative (bottom) torsional motion (rotation along x) measured with the testbed, tension sensors in the tendons and a pose tracking of the upper platform using a camera system. The left plots show the required tendon tension forces whereas the right plots show the change of orientation.

to enable a torsional motion long the x-axis and a bending motion. For the torsional motion, tendon 2-5 are actuated, for the bending motion, tendon 1 and 6 are actuated. The position and orientation of the upper platform is measured with a camera tracking system and an active marker target. Each motor possesses an axial force sensor at the end of each slider to measure the applied tendon force. The chosen configuration of six tendons allows for bending along two axes as well as torsion and the applied silicone structure of Shore hardness 30 A. In Fig. 11, measurements for an induced torsion are depicted. It can be observed that by tensioning tendon 3 and 5 equally, a positive torsional motion about the x-axis is induced (top two diagrams). Due to the symmetric arrangement, the a bending motion is not induced sin the tendon tensions counterbalance each other. For a negative torsional motion, tendon 2 and 4 need to be tensioned equally which can be seen in Fig. 11 in the two bottom diagrams. Non-actuating tendons are controlled in force-control mode ensuring a preset pretension of 20 N.

In Fig. 12 measurements for induced bending motions are shown. Here, tendon 1 induces a bending in one direction and tendon 6 into the other (tendon 1 and 6 are opposing each other). Due to the location of tendon 1 and 6 in the current configuration, the bending results in a coupled motion about the y- and z-axis. However, other placement of the tendons or a coupled control of several tendons would result in decoupled motion in y and z directions.

IV. Future challenges

In the present paper, a platform for experimental research has been introduced. The ultimate goal when designing this platform was to establish a benchmark hardware system with which methods and algorithms can be tested and compared regarding e.g. accuracy, performance or computation time. Beyond that, new

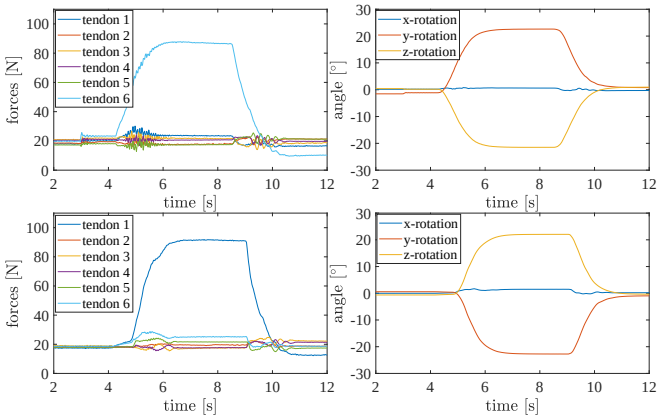

Fig. 12: Positive (top) and negative (bottom) bending motion measured with the testbed, tension sensors in the tendons and a pose tracking of the upper platform using a camera system. The left plots show the required tendon tension forces whereas the right plots show the change of orientation.

concepts for tendon actuation or sensor systems can be tested and compared. In particular, four research areas can be treated with the proposed open source platform and we see the following research challenges arising.

A. Design

As emphasized in Section III, the routing of tendons has major influence on the achievable workspace of the upper platform. As no fundamental or structured work is available which does this, neither in simulations nor in experiments, we formulate this future challenge to find out about the influence of the geometry of the tendon routing w.r.t. the achievable workspace.

Furthermore, the geometric properties of the continuum structure influence its deformation, and therefore, its motion capabilities. Even complex geometric structures can be easily manufactured by 3D-printed molds which is highly beneficial. However, their performance in terms of mechanical stability and workspace is not yet understood well and still needs to be investigated further.

B. Modeling and identification

The design of the testbed is suited to validate static and dynamic models for such systems. Usually, either rigorous models of such systems are used e.g. [13], or essentially reduced models are utilized with lower computational demands suited for model-based control, e.g. [10]. A simulative comparison of different modeling techniques regarding accuracy, computation performance, and potential use cases have been recently performed in [24] which can be complemented effectively with an experimental study performed on the introduced open source tendon-driven continuum mechanism platform.

The design of the pulley swing, described in Section II-D yields a more involved mechanical model to account for the interaction of the tendon, the pulleys, and the associated motion. As a purely geometric problem, this needs to be incorporated in the modeling approach as the motion of the pulleys are also required to build the Jacobian matrix relations from tendon forces to generalized torques of the continuum mechanism.

C. State estimation

In the field of state estimation it is required to estimate the position and orientation of the upper platform. The approach [8] on a similar platform fuses the tendon length measurements of the actuators with the data of an IMU integrated in the upper platform.

Here, two major directions for future estimation concepts can be accounted for with the proposed testbed. The first direction is to develop novel concepts, e.g. model-free or model-based, using the existing sensors (IMU, OPEN-CR board) and the tendon positions of the actuators. The second direction would be to develop and integrate new sensors which can be integrated in such systems and compare them with existing estimation algorithms.

D. Control

Model-based or model-free control approaches for soft robots can be found in the literature [12]. However, as introduced earlier, usually very specific problems are solved originating from the peculiarities of the hardware or robots deployed. With the current platform, control algorithms could be benchmarked as the underlying hardware is exchangeable. In addition, metrics with which these controllers can be assessed are missing which is a relevant research topic for soft robot control.

Recently a model-based controller, which specifically treats the underactuation, has been proposed [9]. In comparison to that, a model-free approach using reinforcement learning [23] was implemented on the same system. Due to their individual capabilities and drawbacks, a combination of both directions might be advantageous. One way would be, for example, to use iterative learning control [7] to improve the trajectory tracking performance.

V. Summary

The present paper introduced an open source tendon-driven continuum mechanisms to make research methods transferable and reproducible. This kind of experimental benchmarking is in line with current trends in the robotics community [3], [24].

The research platform was designed to be mechanically reliable and robust since e.g. all pulleys are equipped with ball bearings or the hard-soft interface was designed and experimentally verified to be capable of withstanding high loading conditions. Here, the experimental verified interface design of the hard and the soft component is emphazised in this work being a crucial part for the stability of the mechanism. To investigate the workspace of tendon-driven continuum mechanisms, the

tendon loading can be easily changed by several different mounting spots of the pulleys. To actuate the continuum mechanism and sense the resulting motion, off-the-shelf sensors and actuators are proposed and their necessary mountings are described. However, also custom actuators can be used due to the platforms modularity.

In summary, the key features researchers should incorporate are the versatile upper/lower platform to enable the modification of the pulley arrangement, the mechanically robust pulley swing with low friction, the interface design of the soft and the hard component to ensure a firm interconnection. To inlcude other continuums of cylindrical cross sections, the same interface design as suggested in Section II-C can be used. A change in the cross sectional shape can be realized as well, whereas a corresponding change of the shape of the interface is required.

Initial experiments show motion capability of the proposed research platform and the paper concludes by identifying future research challenges for this platform.

ACKNOWLEDGMENT

This research has been funded by the German Research Foundation (DFG), grant number 405032572, as part of the priority program 2100 Soft Material Robotic Systems.

References

[1] A. Albu-Schäffer, S. Haddadin, C. Ott, A. Stemmer, T. Wimböck, and G. Hirzinger. The dlr lightweight robot: design and control concepts for robots in human environments. *Industrial Robot*, 2007.

[2] BCN3D. Bcn3d moveo: A fully open source 3d printed robot arm. `https://www.bcn3d.com/bcn3d-moveo-the-future-of-learning-robotic-arm/`. Accessed: 2021-10-15.

[3] F. Bonsignorio. A new kind of article for reproducible research in intelligent robotics [from the field]. *IEEE Robotics & Automation Magazine*, 24(3):178–182, 2017.

[4] J. Burgner-Kahrs, D. C. Rucker, and H. Choset. Continuum robots for medical applications: A survey. *IEEE Transactions on Robotics*, 31(6):1261–1280, 2015.

[5] A. B. Clark, V. Mathivannan, and N. Rojas. A continuum manipulator for open-source surgical robotics research and shared development. *IEEE Transactions on Medical Robotics and Bionics*, 3(1):277–280, 2020.

[6] S. Cousins. Ros on the pr2 [ros topics]. *IEEE Robotics & Automation Magazine*, 17(3):23–25, 2010.

[7] C. Della Santina, M. Bianchi, G. Grioli, F. Angelini, M. Catalano, M. Garabini, and A. Bicchi. Controlling soft robots: balancing feedback and feedforward elements. *IEEE Robotics & Automation Magazine*, 24(3):75–83, 2017.

[8] B. Deutschmann, M. Chalon, J. Reinecke, M. Maier, and C. Ott. Six-dof pose estimation for a tendon-driven continuum mechanism without a deformation model. *IEEE Robotics and Automation Letters*, 4(4):3425–3432, 2019.

[9] B. Deutschmann, A. Dietrich, and C. Ott. Position control of an underactuated continuum mechanism using a reduced nonlinear model. In *56th Annual Conference on Decision and Control*, pages 5223–5230. IEEE, 2017.

[10] B. Deutschmann, T. Liu, A. Dietrich, C. Ott, and D. Lee. A method to identify the nonlinear stiffness characteristics of an elastic continuum mechanism. *IEEE Robotics and Automation Letters*, 3(3):1450–1457, 2018.

[11] S. R. Eugster and B. Deutschmann. A nonlinear timoshenko beam formulation for modeling a tendon-driven compliant neck mechanism. *PAMM*, 18(1), 2018.

[12] T. George Thuruthel, Y. Ansari, E. Falotico, and C. Laschi. Control strategies for soft robotic manipulators: A survey. *Soft robotics*, 5(2):149–163, 2018.

[13] S. Grazioso, G. Di Gironimo, and B. Siciliano. A geometrically exact model for soft continuum robots: The finite element deformation space formulation. *Soft robotics*, 6(6):790–811, 2019.

[14] D. P. Holland, E. J. Park, P. Polygerinos, G. J. Bennett, and C. J. Walsh. The soft robotics toolkit: Shared resources for research and design. *Soft Robotics*, 1(3):224–230, 2014.

[15] Kaupo. Dragon skin. `https://www.kaupo.de/shop/SILIKONKAUTSCHUK-addition/DRAGON-SKIN-SERIE/`. Accessed: 2021-10-15.

[16] Kaupo. Ease release agent. `https://www.kaupo.de/shop/VERSIEGLER-TRENNMITTEL/TRENNMITTEL/Ease-Release-200-1-Trennmittel.html`. Accessed: 2021-10-15.

[17] Kaupo. Solaris primer/1. `https://www.kaupo.de/shop/SILIKONKAUTSCHUK-addition/SOLARIS/Solaris-Primer-1.html?listtype=search&searchparam=primer`. Accessed: 2021-10-15.

[18] Linmot. Linear motors. `https://linmot.com/products/linear-motors/`. Accessed: 2021-10-15.

[19] A. K. Mishra, E. Del Dottore, A. Sadeghi, A. Mondini, and B. Mazzolai. Simba: Tendon-driven modular continuum arm with soft reconfigurable gripper. *Frontiers in Robotics and AI*, 4:4, 2017.

[20] L. U. Odhner, L. P. Jentoft, M. R. Claffee, N. Corson, Y. Tenzer, R. R. Ma, M. Buehler, R. Kohout, R. D. Howe, and A. M. Dollar. A compliant, underactuated hand for robust manipulation. *The International Journal of Robotics Research*, 33(5):736–752, 2014.

[21] I. of Robotics and Mechatronics. Open source tendon-driven continuum mechanism. `https://github.com/DLR-RM/TendonDrivenContinuum`. Accessed: 2021-10-31.

[22] Poppy. Open source platform for the creation, use and sharing of interactive 3d printed robots. `https://www.poppy-project.org/en/`. Accessed: 2021-10-15.

[23] A. Raffin, J. Kober, and F. Stulp. Smooth exploration for robotic reinforcement learning. In *5th Annual Conference on Robot Learning*, 2021.

[24] P. Rao, Q. Peyron, S. Lilge, and J. Burgner-Kahrs. How to model tendon-driven continuum robots and benchmark modelling performance. *Frontiers in Robotics and AI*, 7:223, 2021.

[25] J. Reinecke, B. Deutschmann, and D. Fehrenbach. A structurally flexible humanoid spine based on a tendon-driven elastic continuum. In *International Conference on Robotics and Automation*, pages 4714–4721. IEEE, 2016.

[26] S. Robotics. Stanford pupper: An inexpensive & open-source quadruped robot. `https://stanfordstudentrobotics.org/pupper`. Accessed: 2021-10-15.

[27] Robotis. Servomotor dynamixel xh430-w210-r. `https://www.generationrobots.com/de/402541-servomotor-dynamixel-xh430-w210-r.html`. Accessed: 2021-10-15.

[28] U. Robots. Universal robots ur3e. `https://www.universal-robots.com/de/produkte/ur3-roboter/`. Accessed: 2021-10-15.

[29] H. University and T. C. Dublin. Soft robotics toolkit. `https://softroboticstoolkit.com/`. Accessed: 2021-10-15.

[30] Wacker. Elastosil silicone glue m4601 a/b. `https://www.wacker.com/h/de-de/siliconkautschuk/raumtemperaturvernetzender-siliconkautschuk-rtv-2/elastosil-m-4601-ab/p/000018458`. Accessed: 2021-10-15.

[31] Q. Zhao, K. Nakajima, H. Sumioka, H. Hauser, and R. Pfeifer. Spine dynamics as a computational resource in spine-driven quadruped locomotion. In *International Conference on Intelligent Robots and Systems*, pages 1445–1451. IEEE, 2013.

[32] Zwickroell. Testing machines and testing systems for metals. `https://www.zwickroell.com/products/static-materials-testing-machines/universal-testing-machines-for-static-applications/tensile-tester/`. Accessed: 2021-10-15.